The Ultimate Detection Capability of Diversely Polarized Antenna Arrays using Higher Order Statistics

Supawat Supakwong[*1], Non-member

ABSTRACT

The use of diversely polarized antennas in an array system can significantly improve the overall's array performance. However, its capability does not get utilized to its full potential when the conventional array processing methods are based on the second-order statistic of received signal. The use of higher-order statistic in signal processing is presented in this work. The performance enhancement is evaluated in terms of an array detection that represents the system ability to correctly determine the total number of sources present in an environment. The analysis uses the differential geometry as a tool to analyze the geometrical shape of the corresponding diversely polarized manifold for different orders of statistic. The manifold's intrinsic parameter is then used for the derivation of the detection's lower bound. The theoretical framework is supported by computer simulations to examine the detection capability for various types of antenna arrays with different orders of statistic.

Keywords: Higher-order statistics, Diversely-polarized antennas, Detection, Array manifold

1. INTRODUCTION

In a conventional array system context, an array consisting of uniformly polarized antennas is operated in a multi-source environment. The received signal vector that represents a superposition of individual sources is then processed using the second-order statistic to extract information of interest. This standard framework has long been employed since the early days of array processing [1]. However, its capability does not get utilized to its full potential due to several factors.

First, the system of this type assumes that all sources are transmitted with the same polarization state, and it is perfectly aligned with respect to the orientation of the antennas. This assumption is hardly satisfied in practice. As a result, the polarization mismatch is treated as part of the channel fading.

Manuscript received on May 27, 2015 ; revised on July 04, 2015.

* The authors are with Department of Electrical and Computer Engineering, Faculty of Engineering, Thammasat University, Klong Luang, Pathumthani, Thailand Email: supawat@engr.tu.ac.th[1].

With the advancements in antenna technology nowadays, specialized antennas that can measure multiple components of the electromagnetic wave are commercially available. For example, a vector sensor in [2] can measure all six electromagnetic components of the incident wavefield from a single spatial location. The array performance is significantly improved due to additional information that allows sources to be distinguished on the basis of polarization [3-5]. In addition, there are distributed vector sensors that can measure partial components of the electromagnetic field. For instance, a tripole antenna contains a set of three mutually perpendicular dipoles that can measure three electric field components. A loop triad antenna consists of a set of three identical orthogonally oriented magnetic loops that can measure three magnetic field components. The performance of these distributed vector sensors is varied based on the number of electromagnetic field components the antenna can measure. This comes as a trade-off between the array performance and the computational complexity.

Another limitation factor is due to the use of conventional array processing methods that focus on the received signal's second-order statistic. In spite of providing a high-resolution performance, the methods suffer with several drawbacks. These include the limited number of sources, the system degradation due to Gaussian noise, and the inability to process non-Gaussian signals. Array processing techniques based on a higher-order statistic (HOS) have been proposed to overcome this limitation [6-8]. This is specifically helpful for digital communications where the signals are non-Gaussian.

The purpose of the work presented herein is to assess the performance enhancement of diversely polarized antenna arrays when a HOS of the received signal vector is employed. This is particularly different from a majority of the work [9-12] that has focused on uniformly polarized arrays. In particular, the array performance in terms of the detection capability shall be evaluated. The term "array detection" used in this context refers to the ability of an array to correctly estimate the number of sources. In general, this can be calculated from the dimensionality of the noise subspace [13-14]. However, in the presence of noise and a limited number of samples, it is more difficult to precisely estimate. The ability to

detect the presence of closely-located sources defines an ultimate array detection [15].

From the differential geometry perspective, the studies in [15] investigated the geometrical shape of an array manifold (the locus of all manifold vectors over the set of signal parameters). It showed a direct impact of manifold's intrinsic properties on the overall's array performance such as the Cramer Rao's lower bound (CRB), and the array's detection and resolution. Consequently, the concept of array manifold has been used in a number of array processing applications. These include subspace-type direction-finding algorithms, superresolution array design, modelling error analysis, and the presence of manifold ambiguities. For instance, in [16], the impact of antenna positioning on the array detection capability was investigated from the differential geometry perspective. In an array consisting of vector sensors, it is interested to find (1) an optimum vector sensor placement that can maximize the prescribed detection performance, and (2) the importance of individual antennas in the array that contributes to the overall performance. In [17], the presence of manifold ambiguity in diversely polarized antenna array was investigated. This undesirable incident occurs when diversely polarized manifold vectors corresponding to the sources are linearly dependent. This results in spurious peaks in the direction-finding spectrum. The use of medium substrate was proposed to effectively break down the linear dependence. In both [16] and [17], the framework was based on the analysis of the second-order diversely polarized manifold. Meanwhile, in [18], the performance enhancement of a linear uniformly-polarized antenna array was examined when the fourth-order of statistic is employed. The result was based on the analysis of a (single-parameter) manifold "curve".

In contrast, the work presented herein examines the HOS performance of a diversely polarized antenna array in the presence of sources impinging from any direction in the space and in arbitrary polarization. To assess the detection capability of this array type, it involves the analysis of four-parameter diversely polarized manifold characterized as a function of direction and polarization parameters. The geometrical visualization of this manifold is rather difficult to describe. Consequently, the differential geometry plays an important role in characterizing the array manifold. The manifold's intrinsic parameters are later used to derive the detection's lower bound.

An organization for the rest of the paper is given as follows. In the next section, the signal modelling and problem formulation are first presented. Then, the differential geometry is proposed in Section 3 to investigate the geometric properties of the associated four-parameter HOS diversely polarized manifold, before proceeding to derive the array's detection capability. The theoretical framework is supported by computer simulations in Section 4 to examine the detection capability for various types of antenna arrays and with different orders of statistic, followed by a conclusion in Section 5.

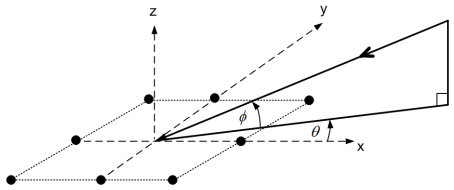

Fig. 1: *A coordinate system of a planar array of vector sensors operated in the presence of an incoming source from an azimuth-elevation* (θ, ϕ).

2. PROBLEM FORMULATION

Consider an array system consisting of N antennas, located at $\mathbf{r} = [\underline{r}_x, \underline{r}_y, \underline{r}_z]^T \in \mathcal{R}^{3\times N}$, measured in half wavelengths. The array is operated in the presence of a single source from an azimuth-elevation (θ, ϕ), where $\theta \in [0, 360^\circ)$ is measured anti-clockwise from the positive $x-$axis, and the elevation $\phi \in [0, 90^\circ)$ is measured anti-clockwise from the $x-y$ plane, as shown in Figure 1. A spatial manifold vector $\underline{\mathbf{a}}(\theta, \phi) \in \mathcal{C}^{\mathrm{N}}$ that corresponds to the array complex response, is given by

$$\underline{\mathbf{a}}(\theta, \phi) = \exp\left\{-j\mathbf{r}^T(\theta, \phi)\right\} \ , \tag{1}$$

where $(\theta, \phi) = \pi\ [\cos\theta\cos\phi,\ \sin\theta\cos\phi,\ \sin\phi]^T \in \mathcal{R}^3$ is the wave-number vector pointing toward the emitter at (θ, ϕ) .

Suppose the array is configured with vector sensors. Hence, each antenna can measure all six electromagnetic components of the wavefield. That is, three electric field components (E_x, E_y, E_z) along the $x-, y-$, and $z-$ coordinates, and three components of the magnetic field (H_x, H_y, H_z) . The field component vector $\underline{q} \in \mathcal{C}^6$ is given by

$$\underline{q} = [E_x, E_y, E_z, H_x, H_y, H_z]^T \ , \tag{2}$$

which can be expressed as

$$\underline{q}(\underline{\Theta}) = \begin{pmatrix} -\sin\theta & -\cos\theta\sin\phi \\ \cos\theta & -\sin\theta\sin\phi \\ 0 & \cos\phi \\ \cos\theta\sin\phi & -\sin\theta \\ \sin\theta\sin\phi & \cos\theta \\ -\cos\phi & 0 \end{pmatrix} \begin{pmatrix} \cos\gamma \\ \sin\gamma\, e^{j\eta} \end{pmatrix} \ , \tag{3}$$

with the polarization parameters $\gamma \in [0^\circ, 90^\circ)$ and $\eta \in [-180^\circ, 180^\circ)$ denote the auxiliary polarization angle and the polarization phase difference respectively. For simplicity, let's define the path's propagation state as $\underline{\Theta} \triangleq [\theta, \phi, \gamma, \eta]^T$.

Consequently, a diversely polarized array manifold vector $\underline{A}(\underline{\Theta}) \in \mathcal{C}^{6N}$ in the presence of a single source is expressed as

$$\underline{A}(\underline{\Theta}) = \underline{\mathbf{a}}(\theta,\phi) \otimes \underline{q}(\underline{\Theta}), \tag{4}$$

where the operator $\otimes$ represents the Kronecker product. In the presence of M narrowband point sources with signal parameters $\underline{\Theta}_i$, where $i \in \{1,\ldots,M\}$, the baseband received signal $\underline{x}(t) \in \mathcal{C}^{6N}$ is a superposition of individual signals, given by

$$\underline{x}\,(t) = \sum_{i=1}^{M} \underline{A}\,(\Theta_i)\, m_i\,(t) + \underline{n}\,(t)\,, \tag{5}$$

with $m_i(t)$ denotes the zero-mean non-Gaussian complex variable of the i^{th} source and $\underline{n}(t)$ is an additive white Gaussian noise vector with zero mean and variance σ^2.

The standard array processing methods exploit the second-order statistic $\mathbb{R}_{xx}$ of $\underline{x}(t)$, where

$$\mathbb{R}_{xx} = \sum_{i=1}^{M} c_{2,m_i} \underline{A}(\underline{\Theta}_i)\underline{A}^H(\underline{\Theta}_i) + \sigma^2 \mathbb{I}_{6N}, \tag{6}$$

with c_{2,m_i} denotes the second-order autocumulant of the message $m_i(t)$, $\mathbb{I}_{6N}$ is a $6N-$dimensional identity matrix, and $(.)^H$ is the Hadamard operation(conjugate-transpose).

On the other hand, the $2q-$HOS array processing methods, where $q > 1$, exploit the information contained in the circular covariance matrix $\mathbb{C}_{2q,x}$ of

$$\begin{aligned}\mathbb{C}_{2q,x}\,(l) = \sum_{i=1}^{M} c_{2q,m_i} \left[\underline{A}(\underline{\Theta}_i)^{\otimes l} \otimes (\underline{A}(\underline{\Theta}_i)^{*\otimes(q-l)}\right] \\ \times \left[(\underline{A}(\underline{\Theta}_i)^{\otimes l} \otimes (\underline{A}(\underline{\Theta}_i)^{*\otimes(q-l)}\right]^H,\end{aligned} \tag{7}$$

where c_{2q,m_i} denotes the $2q-$ order circular autocumulant of $m_i(t)$ and $(.)^*$ is the complex conjugation. In addition, the vector $\underline{A}(\underline{\Theta})^{\otimes l} \in \mathcal{C}^{6Nl}$ is defined as the $l-$folded Kronecker products of the manifold vectors $\underline{A}(\underline{\Theta}_i)$ i.e.

$$\underline{A}(\underline{\Theta}_i)^{\otimes l} \triangleq \underbrace{\underline{A}(\underline{\Theta}_i) \otimes \underline{A}(\underline{\Theta}_i) \otimes \ldots \otimes \underline{A}(\underline{\Theta}_i)}_{l \text{ terms}}. \tag{8}$$

In addition, the integer $0 \le l \le q$ denotes an arrangement of the circular covariance matrix $\mathbb{C}_{2q,x}(l)$. The study in [8] derived a condition to show that the array performance shall be optimized when the integer l satisfies the condition,

$$l = \begin{cases} q/2, & \text{if} q \text{ even}, \\ (q+1)/2, & \text{if} q \text{ odd}. \end{cases} \tag{9}$$

It is seen that the $2q-$order circular cumulant matrix $\mathbb{C}_{2q,x}$ in Equation (7) can be viewed as being the second-order covariance matrix $\mathbb{R}_{xx}$ in Equation (6) with an effective manifold vector $\underline{A}_e(\underline{\Theta})$ given by

$$\underline{A}_e(\underline{\Theta}_i) \triangleq \underline{A}(\underline{\Theta}_i)^{\otimes l} \otimes \underline{A}(\underline{\Theta}_i)^{*\otimes(q-l)}. \tag{10}$$

This virtual array concept, properly described in [8], proves to be essential in understanding the significance of the higher-order statistics. It provides an insight into the mechanism of HOS methods from the traditional second-order statistic perspective.

3. IMPROVING THE ARRAY DETECTION USING HIGHER-ORDER STATISTIC

In this section, the geometrical property of the corresponding four-parameter diversely polarized array manifold with respect to a higher order statistic shall be addressed. The differential geometry is employed as a tool for this analysis. Then, the ultimate array detection that represents the performance's lower bound on the system's ability to determine the number of sources is derived.

3.1 Differential geometry of HOS diversely polarized manifold

From Equation (10), it is seen that the $2q-$order circular covariance matrix $\mathbb{C}_{2q,x}$ can be written in terms of the effective manifold vector $\underline{A}_e(\underline{\Theta})$ expressed as a function of the direction-of-arrival (θ,ϕ) and its polarization (γ,η). Subsequently, the locus of these effective manifold vectors $\underline{A}_e(\underline{\Theta})$ over the set of signal parameters defines the four-parameter effective HOS diversely polarized manifold $\mathcal{V}$. That is,

$$\mathcal{V} = \left\{\underline{A}_e(\theta,\phi,\gamma,\eta) \in \mathcal{C}^{6Nl}, \forall(\theta,\phi,\gamma,\eta) \in \Omega\right\}, \tag{11}$$

where the field-of-view is restricted to

$$\begin{aligned}\Omega = \{(\theta,\phi,\gamma,\eta) : \theta \in [0^\circ, 360^\circ)\,, \phi \in [0^\circ, 90^\circ]\,, \\ \gamma \in [0^\circ, 90^\circ]\,, \eta \in [-180^\circ, 180^\circ)\}\,.\end{aligned} \tag{12}$$

This manifold $\mathcal{V}$ may be viewed as a geometrical object embedded in a $6Nl-$dimensional complex space. Keep in mind that different order of statistic will result in a completely different array manifold and is embedded in a different dimensional complex space.

While the detailed description of the manifold $\mathcal{V}$ shall not be shown, one of the most important manifold's intrinsic parameters for our analysis in this paper is the first fundamental coefficient $\mathcal{I}$ that represents the squared distance between points $\underline{A}(\underline{\Theta}_1)$ and $\underline{A}(\underline{\Theta}_2)$ on the manifold. This can be obtained from

$$\mathcal{I} = \underline{d\Theta}^T \mathbb{G} \underline{d\Theta}, \tag{13}$$

where $\underline{d\Theta}$ denotes signal parameter separation between the two sources $(\underline{\Theta}_1)$ and $(\underline{\Theta}_2)$, i.e.

$$\begin{aligned}\underline{d\Theta} &= \underline{\Theta}_2 - \underline{\Theta}_1, \\ &= [\theta_2 - \theta_1, \phi_2 - \phi_1, \gamma_2 - \gamma_1, \eta_2 - \eta_1]^T.\end{aligned} \tag{14}$$

The matrix $\mathbb{G}$ represents the diversely-polarized manifold metric, where

$$\begin{aligned}\mathbb{G} &= \mathrm{Re}\{\mathbb{J}_{jac}^H \mathbb{J}_{jac}\}, \\ &= \begin{pmatrix} g_{\theta\theta}, & g_{\theta\phi}, & g_{\theta\gamma}, & g_{\theta\eta} \\ g_{\phi\theta}, & g_{\phi\phi}, & g_{\phi\gamma}, & g_{\phi\eta} \\ g_{\gamma\theta}, & g_{\gamma\phi}, & g_{\gamma\gamma}, & g_{\gamma\eta} \\ g_{\eta\theta}, & g_{\eta\phi}, & g_{\eta\gamma}, & g_{\eta\eta} \end{pmatrix},\end{aligned} \tag{15}$$

with $\mathbb{J}$ being the Jacobean matrix whose columns contain the tangent vectors,

$$\mathbb{J}_{jac} = \left[\frac{\partial \underline{A}_e}{\partial\theta}, \frac{\partial \underline{A}_e}{\partial\phi}, \frac{\partial \underline{A}_e}{\partial\gamma}, \frac{\partial \underline{A}_e}{\partial\eta}\right] \in \mathcal{C}^{6Nl\times 4}. \quad (16)$$

3.2 The ultimate's array detection capability

In general, the total number of sources in an array environment can be calculated from the estimated dimensionality of the noise subspace. However, in the presence of noise (measured in terms of the signal-to-noise ratio,SNR) and the limited number of sample size L, the dimensionality of the noise subspace is more difficult to compute. Manikas studied the impact of SNR and L on the deviation of the manifold vector in [15]. He subsequently proposed to model these uncertainties as being a sphere embedded around the error-free manifold vector to probabilistically estimate the position of the actual manifold vector. The sphere's radius σ_e is related to the SNR and the number of sample size L, where

$$\sigma_e = \frac{1}{\sqrt{2(SNR\times L)}}. \quad (17)$$

Consider a scenario when an antenna array is operated in the presence of two closely-located sources with the signal parameters $\underline{\Theta}_1$ and $\underline{\Theta}_2$ accordingly. The parameter separation $\underline{d\Theta} = \underline{\Theta}_1 - \underline{\Theta}_2$ is very small, which makes it rather difficult to detect. Suppose the signal powers for both sources are P_1 and P_2 respectively, the ultimate array detection is defined at the point where the two manifold vectors, $\underline{A}_e(\underline{\Theta}_1)$ and $\underline{A}_e(\underline{\Theta}_2)$, are still linearly independent to each other. Geometrically speaking, it is when the two uncertainty spheres just make a contact, as shown in Figure 2. That is

$$\|\underline{A}_e(\underline{\Theta}_1) - \underline{A}_e(\underline{\Theta}_2)\| = \sigma_{e1} + \sigma_{e2}, \quad (18)$$

where $\sigma_{e1} + \sigma_{e2}$ represents the sum of the uncertainty sphere's radii. Since the two sources are closely located, one can approximate the manifold vector $\underline{A}_e(\underline{\Theta}_2)$ in terms of $\underline{A}_e(\underline{\Theta}_1)$ using the first-order Taylor approximation, where

$$\underline{A}_e(\underline{\Theta}_2) = \underline{A}_e(\underline{\Theta}_1 + \underline{d\Theta}) = \underline{A}_e(\underline{\Theta}_1) + \mathbb{J}_{jac}\underline{d\Theta}. \quad (19)$$

Hence, the term on the left-hand side of Equation (18) can be expressed as

$$\begin{aligned}\|\underline{A}_e(\underline{\Theta}_1) - \underline{A}_e(\underline{\Theta}_2)\| &= \|\mathbb{J}_{jac}\underline{d\Theta}\|, \\ &= \sqrt{\underline{d\Theta}^T \mathrm{Re}\{\mathbb{J}_{jac}^H \mathbb{J}_{jac}\}\underline{d\Theta}}, \\ &= \sqrt{\mathbb{G}\underline{d\Theta}^T\underline{d\Theta}}, \\ &= \sqrt{\mathcal{I}}.,\end{aligned}$$

Let's now substitute the expression of the uncertainty sphere in Equation (17) into the right-hand side of Equation (18). Consequently, we obtained the expression of the array detection's lower bound, expressed in the product term of the signal-to-noise ratio, SNR, and a total number of snapshots$L$, as

$$(SNR_1 \times L) = \frac{1}{2\mathcal{I}}\left(1 + \sqrt{\frac{P_1}{P_2}}\right)^2. \quad (20)$$

Note that, the lower bound is inversely proportional to the parameter $\mathcal{I}$, i.e. the squared distance between the two source points on the manifold. This shows the importance of the manifold's intrinsic geometry (in terms of $\mathcal{I}$) on the overall array detection capability.

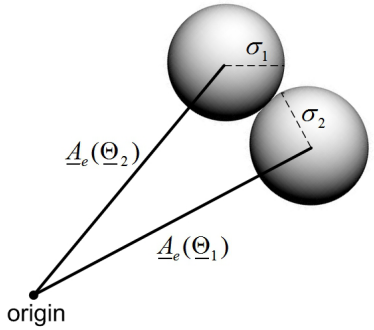

Fig. 2: *The ultimate array detection is defined at the point when the two uncertainty spheres just make a contact.*

4. PERFORMANCE ANALYSIS

The performance analysis is now presented in this section to evaluate the improved array detection capability when the HOS is employed. To proceed, let's first consider a uniform linear array of 3 antennas located at $r_x = [-1, 0, 1]^T$, measured in half wavelength. For the sake of comparison, two types of antennas are used, namely the vertical dipoles and the electromagnetic vector sensors. The array is operated in the presence of two closely-located sources with the azimuth deviation of $\Delta\theta = 1°$, and the same elevation $\Delta\theta = 0°$. Both sources are completely polarized, and transmitted with the linear polarization of $(\gamma, \eta) = (45°, 0°)$. Furthermore, both sources are zero-mean non-Gaussian sources with the quaternary quadrature amplitude modulation (QAM) type, sampled at the sample rate.

Let's consider the intrinsic property of the corresponding $2q-$order manifold. In Figure 3(a) and 4(a), the first fundamental coefficients $\mathcal{I}$ are plotted as a function of the azimuth direction for q=1,2, and 4 for the array of dipoles and vector sensors respectively. Notice how the increasing order of statistic enlarges the parameter $\mathcal{I}$, which represents the squared distance between points $\underline{A}_e(\theta_1, \phi_1, \gamma_1, \eta_1)$ and $\underline{A}_e(\theta_2, \phi_2, \gamma_2, \eta_2)$ on the manifold When the source points are further apart, they are easier to detect.

Table 1: *The average array detection in terms of* $(SNR_1 \times L)$ *for different orders of statistic.*

$(SNR_1 \times L)$	Oder	$\Delta\theta = 1°$	$\Delta\theta = \Delta\gamma = 1°$
Vertical dipoles	$q = 1$	1132.60	868.20
	$q = 2$	377.54	237.40
	$q = 4$	83.90	39.22
Vector sensors	$q = 1$	144.99	195.42
	$q = 2$	20.42	16.29
	$q = 4$	0.28	0.23

Suppose both sources are transmitted with the same power, i.e. $P_1 = P_2 = 1$, then, using Equation (20), the array detection's bound expressed in terms of $(SNR_1 \times L)$ is shown in Figures 3(b) and 4(b) accordingly. Table 1 illustrates the average array detection when it was analyzed over the whole field of view $\theta \in [0°, 360°)$.

Several points can be observed. First, the system enhancement due to the use of HOS is observed. As seen in Figures 3 and 4, the required $(SNR_1 \times L)$ is lowered when the order of statistics $2q$ is increased. For example, in Table 1, when a vector sensor array is operated, the average $(SNR_1 \times L)$ is reduced from 20.42 to 0.28, for $q = 2$ and $q = 4$ accordingly. In addition, the array detection performance when using vector sensors, as compared to the use of vertical dipoles, is significantly better. This is due to the fact that vector sensors can measure all six components of the electromagnetic field; hence, the observability is maximized.

Suppose now that the two sources also have slightly different in the polarization with $\Delta\gamma = \gamma_2 - \gamma_1 = 1°$, in addition to the angular separation of $\Delta\theta = 1°$. The array detection for this scenario when averaging over the field-of-view is shown in the last column of Table 1. Comparing to the first scenario when both sources have the same polarization, it is seen that the detection capability is improved. This is because the difference in signal polarization can add an extra degree of signal discrimination, which allows sources to be detected on the basis of polarization.

Not only the detection capability that is improved when using HOS, the array performance in terms of the Cramer Rao lower bound (CRB) is also enhanced. The CRB represents a lower bound on the error covariance matrix of an angular estimate. Expressed in terms of the curve's geometrical property, in case of a single emitter, the CRB is found from [15],

$$CRB\left[\theta\right] = \frac{1}{2\left(SNR \times L\right)\dot{s}\left(\theta\right)^2},$$

where $\dot{s}\left(\theta\right)$ denotes the rate-of-change of arclength for the corresponding polarized manifold curve. As shown in Figure 5, notice the CRB performance enhancement from the vector sensor array for different orders of statistic.

Let's examine the accuracy of the array detection based on 50,000 independent Monte-Carlo runs. The array setting remains the same, where a three-element uniform linear array with half wavelength apart is employed. Suppose the array is operated in the presence of two sources with quaternary QAM signal type,where

$$\underline{\Theta}_1 = (\theta_1, \phi_1, \gamma_1, \eta_1)^T = (30°, 0°, 30°, 0°),$$
$$\underline{\Theta}_2 = (\theta_2, \phi_2, \gamma_2, \eta_2)^T = (33°, 0°, 35°, 0°).$$

The two sources were slightly apart with $\Delta\theta = 3°$. Both were transmitted in a linear polarization state with small deviation in the orientation, where $\Delta\gamma = 5°$. The noise power is $\sigma^2 = 0.1$,and different numbers of snapshots were examined $L = \{10, 30, \ldots, 170\}$. The number of detected sources is estimated using Akaike Information Criterion (AIC) [13] based on the eigen-decomposition of the circular covariance matrix $\mathbb{C}_{2q,x}$ and is determined from the estimated dimensionality of the noise subspace. The accuracy rate is computed based on the total number of correct detection over 50,000 Monte-Carlo runs.

The result is shown in Figure 6, where several points can be addressed. As expected, the accuracy rate of an array detection is improved when increasing the statistical order q, increasing the number of sample size L and when the diversely polarized antennas were used. It should be noted that the array detection performs very poorly with the accuracy rate less than 10% when the dipole antennas were employed with the order q =1 and 2. This shows that the detection performance gets strongly affected when the sources are poorly separated. In the presence of a limited number of samples, the array indeed sees these two incoming plane waves as it is from a single source. On the other hand, the vector sensor array with HOS can accurately distinguish the presence of both sources. It is seen that there are cases when we cannot find a single error detection from the total of 50,000 runs.

Next, let's examine the array detection capability in a two-dimensional array. Consider planar arrays of N =9 vector sensors, arranged in three different configurations, namely the circular, triangular, and crossed arrays, as shown in Figure 7, with the positions listed in Equation (21)-(23) (bottom of this page).

$$[\underline{r}_x, \underline{r}_y]^T_{circular} = \begin{pmatrix} 2.00, 1.53, 0.35, -1.00, -1.88, -1.88, -1.00, 0.35, 1.53 \\ 0.00, 1.29, 1.97, 1.73, 0.68, -0.68, -1.73, -1.97, -1.29 \end{pmatrix} \quad (21)$$

$$[\underline{r}_x, \underline{r}_y]^T_{triangular} = \begin{pmatrix} -2.00, -0.67, 0.67, 2.00, 1.33, 0.67, 0.00 - 0.67, -1.33 \\ -1.15, -1.15, -1.15, -1.15, 0.00, 1.15, 2.30, 1.15, 0.00 \end{pmatrix}$$

$$[\underline{r}_x, \underline{r}_y]^T_{crossed} = \begin{pmatrix} 0.00, 0.71, -0.71, -0.71, 0.71, 1.41, -1.41, -1.41, 1.41 \\ 0.00, 0.71, 0.71, -0.71, -0.71, 1.41, 1.41, -1.41, -1.41 \end{pmatrix}$$

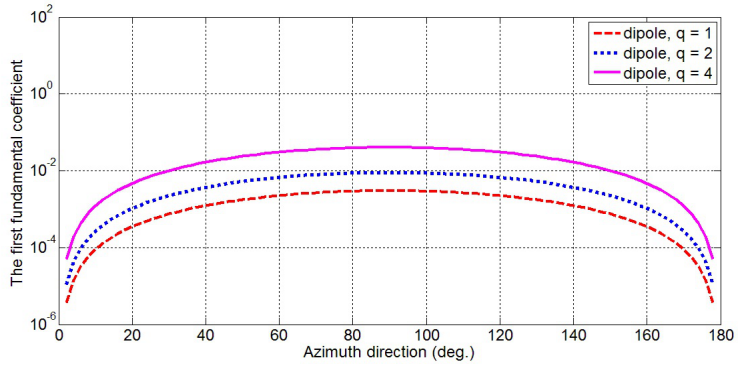

(a)

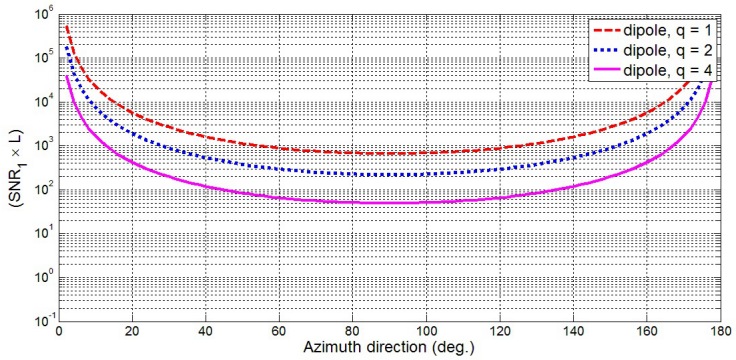

(b)

Fig.3: *A linear array with dipole antennas. (a) the first fundamental coefficient $\mathcal{I}$, and (b) the detection lower bound in terms of $(SNR_1 \times L)$, plotted as a function of azimuth angle for different orders of statistic.*

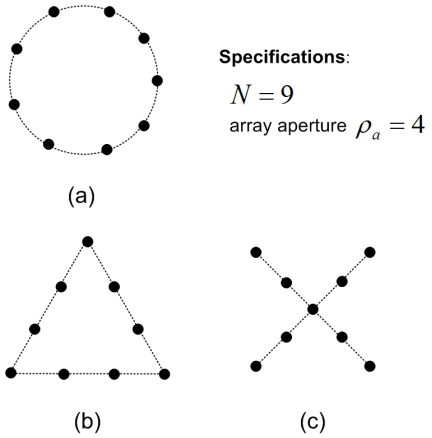

Fig.7: *Configurations of planar arrays with $N = 9$. (a) circular (b) triangular (c) crossed arrays. All arrays have the same aperture.*

The arrays are operated in the presence of two equi-power sources. Two scenarios are considered.

(i) Both sources have the same polarization state with $(\gamma, \eta) = (45°, 0°)$, and the angular separation is $(\Delta\theta, \Delta\phi) = (1°, 1°)$.

(ii) (ii) Sources are different in both the azimuth-elevation direction and the polarization with $\Delta\theta = \Delta\phi = \Delta\gamma = \Delta\eta = 1°$.

The average $(SNR_1 \times L)$ over the whole field-of-view is summarized in Table 2. The performances are assessed using the $2^{nd}-, 4^{th}-$and $8^{th}-$orders of statistics respectively.

Several points can be noted. First, the array enhancement is observed when using a higher-order of statistic. For instance in the circular array, the required $(SNR_1 \times L)$ is decreased from 17.47 to 0.49 and 7.1×10^{-4} respectively when using 4^{th} and 8^{th} orders of statistic accordingly. Furthermore, the array configuration plays a part in the overall array performance. In this example, the circular array is shown to be the optimal choice, followed by the triangle and crossed arrays respectively. Finally, comparing the detection threshold between cases (i) and (ii), it is clear how the additional information of the signal polarization can help in improving the overall's array detection capability.

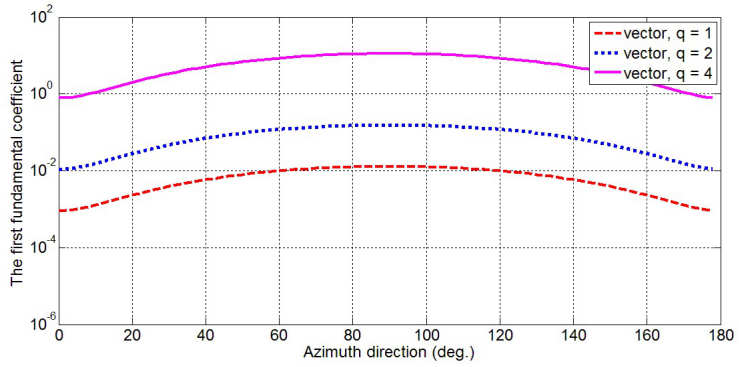

(a)

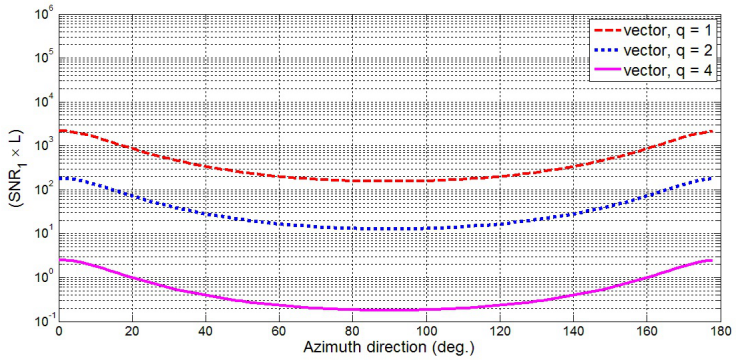

(b)

Fig.4: *A linear array with vector sensors. (a) the first fundamental coefficient $\mathcal{I}$, and (b) the detection lower bound in terms of $(SNR_1 \times L)$, plotted as a function of azimuth angle for different orders of statistic.*

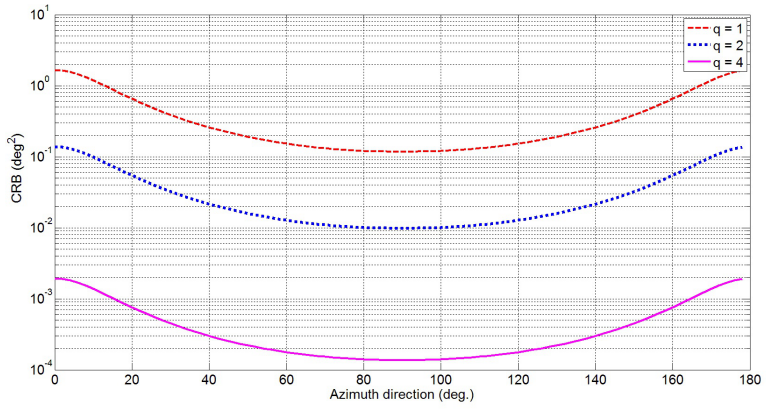

Fig.5: *A linear array with vector sensors. The CRB as a function of azimuth direction, plotted for different orders of statistic.$SNR = 0.01, L = 10, \Delta\theta = \Delta\gamma = 1^\circ$.*

5. CONCLUSION

An ultimate's array detection capabilities based on the use of higher-order statistic in diversely polarized antenna arrays was evaluated in this paper. An array detection's lower bound represents the system ability to determine the number of sources in an environment. This bound is fundamentally related to the geometrical shape of the array manifold, specifically in terms of the first fundamental coefficient $\mathcal{I}$ that represents the squared distance between two points on the manifold. Using the differential geometry as a tool to analyze the corresponding diversely polarized array manifold with respect to different orders of statistics, the performance analysis was presented to evaluate the improved ultimate's array detection capability.

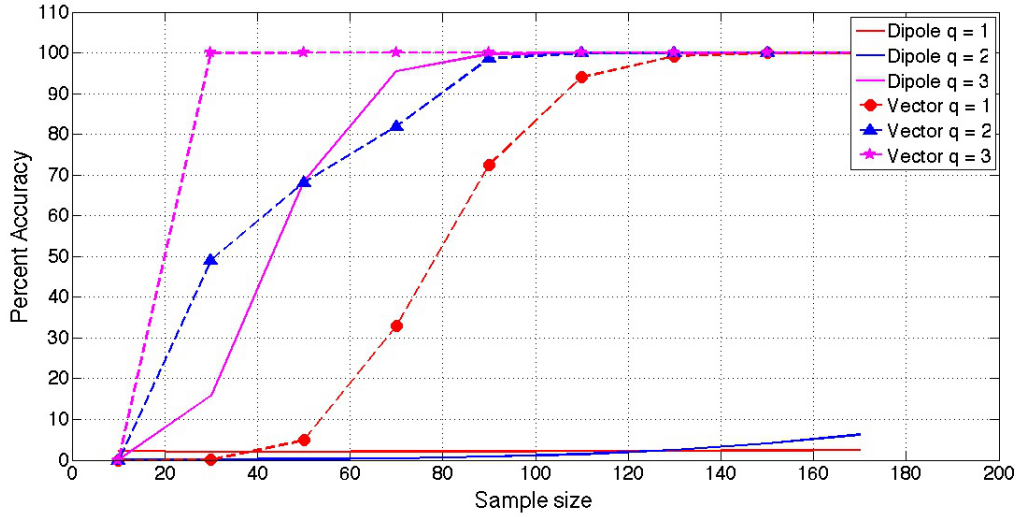

Fig.6: *The array detection accuracy as a function of the number of samples L, plotted for different orders of statistics.*

Table 2: *The average array detection in terms of* $(SNR_1 \times L)$ *for different orders of statistic with the configurations (a) circular (b) triangular (c) crossed arrays.*

$(SNR_1 \times L)$	Oder	$(\Delta\theta, \Delta\phi) = (1°, 1°)$	$(\Delta\theta, \Delta\phi, \Delta\gamma, \Delta\eta) = (1°, 1°, 1°, 1°)$
(a) Circular array	$q = 1$	17.47	15.67
	$q = 2$	0.49	0.44
	$q = 4$	7.1×10^{-4}	7.0×10^{-4}
(b) triangular array	$q = 1$	11.11	11.02
	$q = 2$	0.64	0.57
	$q = 4$	1.0×10^{-3}	9.0×10^{-4}
(c) crossed array	$q = 1$	30.14	25.18
	$q = 2$	0.84	0.71
	$q = 4$	1.3×10^{-3}	1.1×10^{-3}

References

[1] S. Pillai, *Array Signal Processing. Springer-Verlag*, 1989

[2] A. Nehorai, and E. Paldi, "Vector-sensor array processing for electromagneticsource localization," *IEEE Trans. Signal Process.*, vol. 42, no. 2, pp. 376-398, Fab. 1994.

[3] M. R. Andrews, P. P. Mitra, and R. deCarvalho, "Tripling the capacity of wireless communications using electromagnetic polarization," *Nature*, vol. 409, pp. 316-318, 2001.

[4] A.Weiss and, B. Friedlander, "Direction finding for diversely polarized signals using polynomial rooting," *IEEE Trans. Signal Process.*, vol. 41, pp. 1893-1905, May. 1993.

[5] A. Weiss, and B. Friedlander, "Analysis of a signal estimation algorithm for diversely polarized arrays," *IEEE Trans. Signal Process.*, vol. 41, pp. 2628-2638, Aug. 1993.

[6] M.C. Dogan, and J.M. Mendel, "Applications of cumulants to array processing (i) aperture extension and array calibration," *IEEE Trans. Signal Process.*, vol. 43, no. 5, pp. 1200-1216, May. 1995.

[7] M.C. Dogan, and J.M. Mendel, "Applications of cumulants to array processing (ii) non-gaussian noise suppression," *IEEE Trans. Signal Process.*, vol. 43, no. 7, pp. 1663-1676, Jul. 1995.

[8] P. Chevalier, L. Albera, A. Ferreol, and P. Comon, "On the virtual array concept for higher order array processing," *IEEE Trans. Signal Process.*, vol. 53, no. 4, pp. 1254-1271, Apr. 2005.

[9] P. Chevalier, A. Ferreol, and L. Albera, "High-resolution direction finding from higher order statistics: The MUSIC algorithm," *IEEE Trans. Signal Process.*, vol. 54, no. 8, pp. 2986-2997, Aug. 2006.

[10] P. Pal, and P. Vaidyanathan, "Multiple level nested array: An efficient geometry for order cumulant based array processing," *IEEE Trans. Signal Process.*, vol. 60, no. 3, pp. 1253-1269, Mar. 2012.

[11] G. Birot, L. Albera, and P. Chevalier, "Sequential high-resolution direction finding from higher order statistics," *IEEE Trans. Signal Process.*, vol. 58, no. 8, pp. 4144-4155, Aug. 2010.

[12] Wang, F, Cui, and X, Lu, M., "Direction Finding Using Higher Order Statistics Without redundancy," *IEEE Trans. Signal Process.*, vol. 20, no. 5, pp. 495-498, May. 2013.

[13] H. Akaike, "A new look at the statistical model identification," *IEEE Trans. Autom. Control*, vol. 19, pp. 716-723, 1974.

[14] M. Wax, and T. Kailath, "Detection of signals by information theoretic criteria," *IEEE Trans. Acoust., Speech, Signal Process.*, vol. 33, pp. 387-

392, 1985.

[15] A. Manikas, *Differential Geometry in Array Processing.*, London, Imperial College Press, 2004.

[16] S. Supakwong, "Resolving Diversely Polarized Manifold Ambiguity using Planar Substrate Placement," *6th International Symposium on Communications, Control, and Signal Processing*), Athens, Greece, pp 478-481, 2014.

[17] S. Supakwong, "The significance of vector sensor positioning on the array's ultimate detection capability,"*Proceedings of ECTI-CON 2010*, Chiang Mai, Thailand, pp.1272-1276, 2010.

[18] N. Takai, and A. Manikas, "Array manifold properties and performance of higher-order signal subspace techniques,"*in Acoustics, Speech, and Signal Processing, IEEE Int. Conf. on*, pp.666-669, 1993.

Supawat Supakwong He received his Bachelor and Master degrees in 2004 and 2005 respectively from University of Virginia, USA, and his Ph.D. from Imperial College London, UK in 2009, all in electrical engineering. His main research work is in the area of array signal processing and communications.